Available online at www.sciencedirect.com
SCIENCE DIRECT®
Journal of Sound and Vibration 282 (2005) 735–751
JOURNAL OF SOUND AND VIBRATION
www.elsevier.com/locate/jsvi

Investigation into piston-slap-induced vibration for engine condition simulation and monitoring

Z. Geng*, J. Chen

[a]*State Key Lab on Vibration, Shock and Noise, Shanghai Jiao Tong University, Shanghai 200030, PR China*

Received 6 June 2001; accepted 9 March 2004

Abstract

Piston slap is a common impact phenomenon existing in the reciprocating engine. It is also a major cause of the complex transient vibration response related to the impact excitation inside the engine. In order to correlate the piston-slap impact with the slap-induced vibration and consequently find out an effective approach for the engine dynamic behaviour simulation and working condition monitoring, an in-depth investigation from theoretical modelling to experimental verification is made in this paper.

Firstly, the piston-slap phenomenon inside the reciprocating engine is briefly discussed from the viewpoint of engine mechanics. Based upon this, a nonlinear model is developed to simulate the slap-induced vibration response. Using numerical integration procedure, the slap-induced vibration response and its correlation with the inner-cylinder piston-slap impact are reasonably evaluated.

Guided by the simulating results and, by introducing a fast wavelet-packet decomposition and reconstruction algorithm, a specially designed experiment is made to practically measure and extract the slap-induced impact message inside the $6190Z_LC$ diesel engine. Comparison between the simulation and practically measured and reconstructed engine vibration signals verifies the effectiveness and practicality of this approach for more detailed academic research and engineering application.

*Corresponding author. Current address: Advanced Manufacturing Research Centre (AMRC) with Boeing, University of Sheffield, Advanced Manufacturing Park, Wallis Way, Catcliffe, Rotherham S60 5TZ, UK.
E-mail address: zunmin.geng@ntlworld.com (Z. Geng).

0022-460X/$ - see front matter © 2004 Elsevier Ltd. All rights reserved.
doi:10.1016/j.jsv.2004.03.057

Nomenclature

c_1	viscous damping between the piston assembly and piston ring
c_2	viscous damping between the piston and cylinder wall
c_3	viscous damping between the cylinder wall and engine casing
$C_{i,j}$	the ith by jth scale factor of the wavelet-packet
$f(r_i, t)$	the Inner-engine excitation
f_{sm}	sampling frequency
G	high-pass differential-filter of the wavelet-packet
H	low-pass averaging-filter of the wavelet-packet
$h(r_i, t)$	time-varying transfer function from $f(r_i, t)$ to engine casing
k_{11}	contacting stiffness between piston and cylinder wall
k_{12}	linear stiffness between piston and cylinder wall
k_2	linear stiffness from the piston ring
k_3	linear stiffness between the cylinder wall and engine casing
J, J_1, J_2	decomposing layer of the wavelet-packet
l	length of the connecting rod
m_1, m_2	lumped masses of the piston assembly and the cylinder wall
N	sample length of the vibration signal
$N(r_i, t)$	counting variable of the Poisson impacting process
$n(t)$	Gaussian noise
P_c	inner-cylinder combustion force
P_i	inertia force of the piston assembly
P_y	inner-cylinder side-thrust force
r_c	crank radius
$u(t)$	the engine vibration response
V_n	impact intensity of the Poisson process
$w(\tau_n)$	impact waveform of the Poisson process
x_1	transverse vibration displacement of the piston
x_2	transverse vibration displacement of the cylinder wall
$x_p, \dot{x}_p, \ddot{x}_p$	displacement, velocity and acceleration of the piston assembly
τ_n	impact happening time of the Poisson process
Δ	piston clearence
$\lambda = r_c/l$	connecting rod/crank radius ratio.

1. Introduction

It is well known that the periodogram-based signal processing and signature extraction is a useful approach for the vibration analysis and condition monitoring of the rotational machinery [1]. However, until recently, few publications have shown successful applications of this approach to reciprocating engines without specially designed improvements and limitations [2–4]. In order to develop an effective analysing and monitoring approach by using the engine vibration, many efforts have been made in recent years, such as Lyon's SEA method and indirect recovery of the inner-cylinder excitations [2,3], Cempel's vibro-acoustic method [4], etc. Among these approaches, evaluation of the impact excitation inside the engine and its correlation with the engine vibration is gaining more and more attention [5].

As the authors researched [6,7], impact excitations, time-varying transfer properties, severe reverberation and dispersion are important characteristics of the engine vibration. These make its transient response so complex that no significant signature can be directly obtained from its spectrum. A synchronously measured correlation between the inner-cylinder excitation (combustion pressure, I) and vibration response from the cylinder wall (overloaded waveform to view the detailed piston-slap-induced vibration, with the help of transmitting rod as shown in

Fig. 2, transverse and perpendicular to the crankshaft, III) of the 6190Z_LC diesel engine (Jinan engine Ltd., China. Mainly for marine use, 4 strokes, 6 cylinders vertically, cylinder diameters: 190 mm, maximum speed: 3000 rev/min) in its working cycle (Top-Dead-Centre from an electromagnetic sensor, II) is shown in Fig. 1, which presents a clear explanation for this situation. On one hand, it expresses a mutually dependent correlation of the inner-cylinder working process, mechanical system and the vibration response of the engine. On the other hand, because of the widespread mechanical and fluid impacts, severe reverberation and dispersion inside the engine [3,7], this correlation is almost completely submerged in the 'chaotic' response waveform. Obviously, any achievements in locating and identifying this correlation from the complex vibration response will possess significance, both in the engine's performance evaluation and dynamic behaviour analysis, as well as in its working condition monitoring.

As a generalized description and considering the occurrence and intensity of every impact modulated by the relative dynamic relations of the engine, a global expression of the engine vibration has already been concluded by Geng [7] as

$$u(t) = \sum_{i=1}^{m} \int_0^t h(r_i, t-t) f(r_i, \tau\tau) \mathrm{d}t + \sum_{k=1}^{N(t)} V_n w(t) d(t - t_n) + n(t), \tag{1}$$

where $h(r_i, t)$ is the time-varying transfer route from the inner-engine excitation $f(r_i, t)$ $(i = 1, 2, \ldots, m)$; $w(r_j, t_n)$ is the high-frequency impact waveform arrived at time τ_n, enhanced by its intensity V_n and modulated by the unstable inner-cylinder working process, as well as the kinematic relationship of the inner-engine subsystems, with a modulation counting variable $N(r_j, t)$ [3,4,7,9].

According to Eq. (1) and the reciprocating engine's working mechanism, some particular impact waveform $w(r_j, t_n)$ can be located by simulating and identifying its exact arriving time τ_n. Furthermore, the impact waveform $w(r_j, t_n)$ and intensity V_n can be recovered by specially designed signal processing methods. This approach is not only essential for evaluating its dynamic

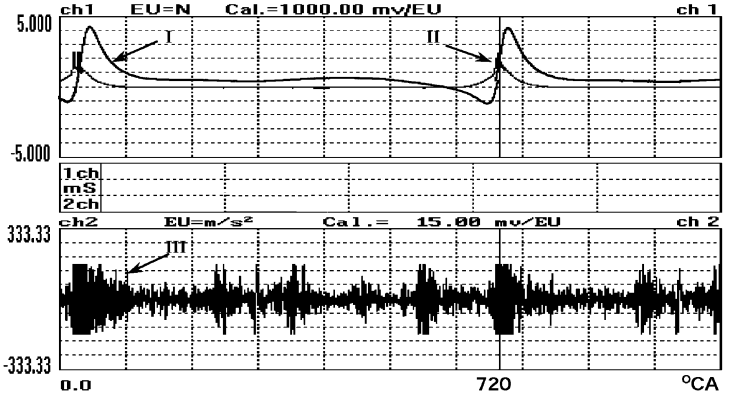

Fig. 1. Basic dynamic correlation in a diesel engine.

behaviour but also important in making the precise diagnosis of the engine's working condition. As an initial aim of this attempt, the following investigation into the piston-slap-induced vibration reveals an effective approach to it.

2. Analysis of the piston-slap phenomenon

Piston slap is a common impact phenomenon existing in the reciprocating engine. It also plays an important role in its transverse vibration (perpendicular to the crankshaft). As briefly shown in Fig. 2, driven by the inner-cylinder combustion pressure, the piston moves along the cylinder with a relatively constant speed mainly maintained by the flywheel. Meanwhile, due to the periodically changing pendular angle of the connecting rod, a periodically changing side-thrust is decomposed from the longitudinally acting combustion pressure and inertial force of the moving piston assembly, which pushes the piston assembly from one side of the cylinder wall skipping onto the other side, so as to induce an unceasing slap impact on the cylinder wall [9]. Predictably, existence of the piston clearance amplifies this impact effect.

Fig. 2 also shows a specially designed test rig for the measurement of the piston-slap impact. In order to directly reach the cylinder wall and pick up the slap-impact message with noise interference to its minimum, solid steel transmitting rods (longitudinal resonance higher than 20 kHz, positioned, respectively, along the crankshaft angle of 180°, 290° and 360°, on both sides of the cylinder wall) and an accelerometer are applied, coupled with the commonly used signal analysing equipments. Along with all the measurements involved in this paper, this test rig is used.

Further investigating the dynamics of the crank–piston system as shown in Fig. 2, mainly maintained by the flywheel, the crankshaft can be taken to be rotating at a uniform speed, i.e., ω is contant. Based upon this assumption, the exact expression for the piston displacement x_p in terms

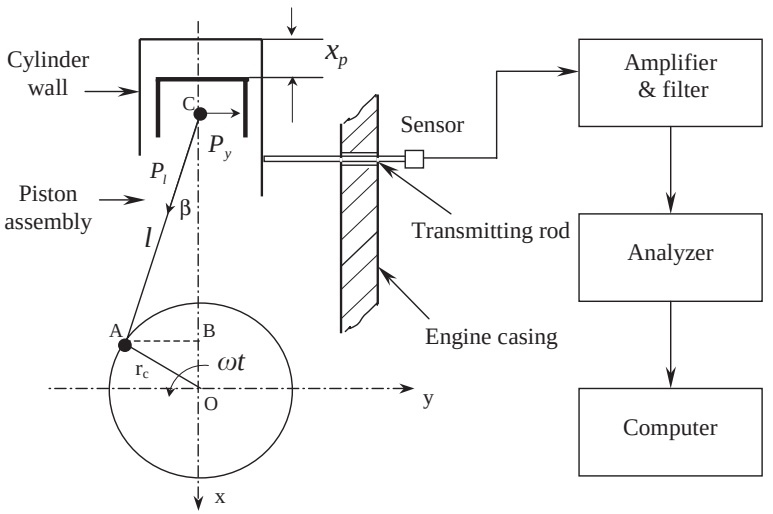

Fig. 2. Crank mechanism and piston-slap measurement scheme.

of the crank angle ωt can be derived as [9]

$$x_p = r_c(1 - \cos\omega t) + l\left(1 - \sqrt{1 - \lambda^2 \sin^2 \omega t}\right), \tag{2a}$$

where $\lambda = r_c/l$, r_c is the crank radius and l is the length of the connecting rod.

Furthermore, Eq. (2a) can be simplifies into its first-term approximation form

$$x_p \approx r_c(1 - \cos\omega t) + \tfrac{1}{2}\lambda^2 \sin^2 \omega t. \tag{2b}$$

The velocity and acceleration follow from the displacement by differentiation:

$$\dot{x}_p = r_c\omega\left[\sin\omega t + \tfrac{1}{2}\lambda \sin 2\omega t\right], \quad \ddot{x}_p = r_c[\cos\omega t + \lambda \cos 2\omega t]. \tag{2c}$$

Based upon the above derivations, the side-thrust force of the piston on the cylinder wall is further decomposed from the longitudinally acting combustion pressure P_c and inertial force of the moving piston assembly $P_i = m_1 r_c \omega^2(\cos\omega t + \lambda \cos 2\omega t)$ (m_1 is the equivalent mass of the piston assembly). Due to the periodically changing pendular angle of the connecting rod, the side-thrust force is also periodically changing, with a periodic term $\sin\omega t/\sqrt{1 + (\lambda \sin\omega t)^2}$, which pushes the piston assembly from one side of the cylinder wall skipping onto the other side. Mathematically, this side-thrust force can be derived as

$$\begin{aligned} P_y &= (P_c - P_i)\lambda \sin\omega t \Big/ \sqrt{1 + (\lambda \sin\omega t)^2} \\ &= [P_c - m_1 r_c \omega^2(\cos\omega t + \lambda \cos 2\omega t)]\lambda \sin\omega t \Big/ \sqrt{1 + (\lambda \sin\omega t)^2}. \end{aligned} \tag{3}$$

By introducing the physical parameters and practically measured inner-cylinder combustion pressure P_c of the 6190Z_LC diesel engine (Fig. 1) into Eq. (3), the side-thrust force can be simulated as shown in Fig. 3. What should be specially mentioned here is that, as for the combined side-thrust force P_y, every time it passes zero and changes direction (from positive to negative, or vice versa) means an occurrence of piston-slap impact on a definite position along the cylinder wall. In this instance, there are 6 slap impacts occurring in its four-stroke working cycle (points A–F in Fig. 3).

Further investigating the simulation results shown in Fig. 3, it is not difficult to find that, with different combination of the combustion pressure and inertia force of the piston assembly, the combined side-thrust force P_y presents a significant change in its waveform and so do the occurrences of the piston-slap impacts. This means, the number of piston-slap impacts as well as the time of occurrence in a working cycle can be taken as potential monitoring indicators of the engine performance and working condition. Apparently, for the same type of engine with the same working parameter setting, one engine with more slap impacts caused by the inertia force will be in a worse performance or working condition than another one with more slap impacts caused by the combustion pressure.

As a further complement of the above analysis, Fig. 4 shows two groups of experiments, respectively, emphasizing the influences from the inertia force (Fig. 4a: no external load; different rotating speeds from 1000 to 2500 rev/min) and combustion force (Fig. 4b: fixed rotating speed 2500 rev/min; different external loads from 0 to 45 Nm). Table 1 also lists the calculated time of

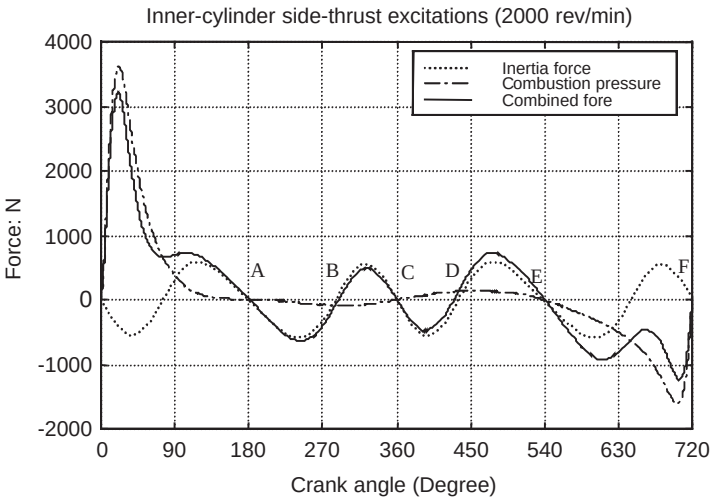

Fig. 3. Composition of the inner-cylinder side-thrust (external load: 0.0 Nm).

impact occurrence, compared with those obtained from the slap-induced vibration response simulation as well as experimentally confirmed ones via the test rig shown in Fig. 2 (to be further discussed in the following paragraphs). As a rough estimation, these results conclude that the side-thrust force as well as the piston-slap impacts, from the waveform to the time of occurrence, is sensitively changing with different combinations of the combustion pressure and inertia force of the piston assembly, and so on, reflecting different performance or working conditions of the engine. From this point, these simulations reveal the necessity of further investigating into the structural transient response caused by the piston-slap impacts, as well as the possibility of applying it to the engine's performance or working condition monitoring.

3. Dynamic modelling

As is mentioned above, existence of the piston clearance amplifies the slap impacting effect, and in turn, the structural response of the cylinder wall caused by these impacts further applies complex influences on the intensities and ocurrences of the practically measured slap-impact messages (e.g., the obvious phase delay listed in Table 1). In order to have a detailed investigation into this situation, a two-degree-of-freedom (tdof) nonlinear model extracted from the practical piston–cylinder system in Fig. 2 is developed in Fig. 5.

In this tdof nonlinear model, the piston assembly is simplified into a lumped mass $m_1 \approx 1.25\,\mathrm{kg}$ for the $6190Z_LC$ diesel engine, referring to its first dof x_1. The piston is held in position by the elastic piston rings between it and the cylinder wall, with stiffness $k_2 \approx 89450.0\,\mathrm{N/m}$. Another coupling between the piston assembly and the cylinder wall is from the piston clearance Δ (for simulation, Δ is set from 0.05 to 1.25 mm), which is the major nonlinear element of the tdof system and the cause of slap impacts. Considering the impacting transient when the piston assembly contacts the cylinder wall over the piston clearance Δ, a nonlinear contacting stiffness element

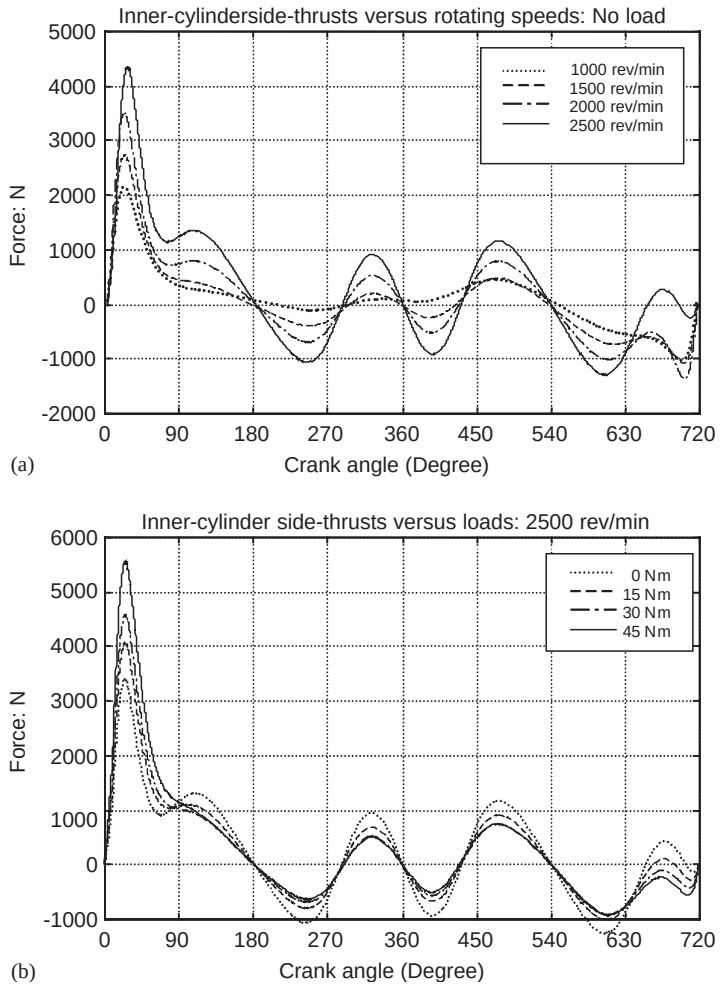

Fig. 4. Side-thrust forces under different working conditions: (a) side-thrust forces under different rotating speeds, (b) side-thrust forces under different external loads.

$k_{11}x^3$ (in this case, the nonlinear stiffness k_{11} is experimentally set as $k_{11} = 0.64 \times 10^9\,\mathrm{N/m^3}$, mainly for the impacting transient), coupled with a linear stiffness $k_{12} = 2.26 \times 10^5\,\mathrm{N/m}$ (during and after the impacting transient), is attached to the connection between the piston assembly and the cylinder wall [8,9].

Further considering the second dof x_2 of the tdof nonlinear model, mainly for simplicity, the cylinder wall assembly is simplified as rigidly constructed along the direction of piston movement (as for the $6190\mathrm{Z_L}$C diesel engine design, actually, along this direction, there are 3 supporting points from the engine casing to the cylinder wall, with lower linear stiffness than the cylinder wall itself and in this case, it can be roughly taken as rigid in this direction), with lumped mass $m_2 \approx 22.65\,\mathrm{kg}$, as well as linear stiffness connection $k_3 = 1.25 \times 10^5\,\mathrm{N/m}$ between the cylinder wall and engine casing through the flexible supporting points.

Table 1
Occurrences of slap-impact and slap-induced vibration response

External load: 0.0 N m				External load: 45.0 N m			
Rotating speed (rev/min)							
1000	1500	2000	2500	1000	1500	2000	2500
Slap-impact and slap-induced response position (crank angle: deg)							
0.0	0.0	0.0	0.0	0.0	0.0	0.0	0.0
(16.5)	(21.0)	(24.5)	(28.0)	(16.5)	(18.5)	(23.0)	(28.0)
[16.0]	[21.0]	[25.0]	[28.0]	[16.5]	[19.0]	[22.5]	[26.5]
198.0	182.5	186.0	186.5	180.0	180.0	180.0	180.0
(239.5)	(242.5)	(246.0)	(254.5)	(242.5)	(246.0)	(254.0)	(258.0)
[236.5]	[242.0]	[244.0]	[248.4]	[235.5]	[240.0]	[242.5]	[246.5]
286.8	287.6	288.8	282.5	295.2	292.5	288.2	286.6
(--)	(--)	(--)	(--)	(321.0)	(321.5)	(324.0)	(326.0)
[--]	[--]	[--]	[--]	[318.5]	[319.0]	[316.0]	[318.0]
--	360.0	360.0	360.0	360.0	360.0	360.0	360.0
(--)	(--)	(--)	(352.0)	(352.5)	(362.5)	(366.0)	(368.0)
[--]	[--]	[--]	[362.0]	[358.0]	[361.0]	[364.0]	[368.0]
--	422.8	429.2	432.2	421.5	420.4	428.0	432.2
(--)	(--)	(455.5)	(465.5)	(446.0)	(460.5)	(458.0)	(468.0)
[--]	[--]	[450.0]	[458.0]	[445.0]	[456.5]	[460.0]	[460.0]
548.0	538.5	540.0	540.0	540.0	540.0	540.0	540.0
(--)	(--)	(611.0)	(618.5)	(581.0)	(584.0)	(588.0)	(586.0)
[--]	[--]	[567.0]	[578.0]	[569.0]	[572.0]	[574.5]	[578.0]
--	--	--	659.9	652.0	659.0	661.0	661.0
(--)	(--)	(--)	(689.5)	(692.0)	(692.5)	(695.0)	(697.5)
[--]	[--]	[--]	[691.0]	[691.0]	[692.0]	[694.0]	[696.0]
--	--	--	689.0	692.0	693.0	696.0	699.0
(--)	(--)	(--)	(--)	(--)	(--)	(--)	(--)
[--]	[--]	[--]	[--]	[--]	[--]	[--]	[--]

'--' : Unidentifiable; ( ), slap-induced response; [ ], experimentally confirmed.

Via experimental modal analysis [3,4], and considering the lubricant's damping effect between the piston assembly and cylinder wall, viscous dampers c_1, c_2 and c_3 ($\zeta_1 = c_1/(2\sqrt{m_1 k_{12}}) = 0.013$, $\zeta_2 = c_2/(2\sqrt{m_1 k_2}) = 0.028$, $\zeta_3 = c_3/(2\sqrt{m_2 k_3}) = 0.011$) are further added to the different dof of this tdof system. Based on this, a corresponding differential equation is derived as [8]:

$$\begin{aligned} &m_1\ddot{x}_1 + c_2(\dot{x}_1 - \dot{x}_2) + k_{12}(x_1 - x_2) = P_y \\ &m_2\ddot{x}_2 + 2c_3\dot{x}_2 + c_2(\dot{x}_2 - \dot{x}_1) + 2k_3x_2 + k_2(x_2 - x_1) = 0, \quad (|x_1 - x_2| \leqslant \Delta) \end{aligned} \tag{4a}$$

$$\begin{aligned} &m_1\ddot{x}_1 + (c_1 + c_2)(\dot{x}_1 - \dot{x}_2) + (k_{12} + k_2)(x_1 - x_2) \\ &\quad + k_{11}(x_1 - x_2)^3 - k_{12}\Delta = P_y \\ &m_2\ddot{x}_2 + 2c_3\dot{x}_2 + (c_1 + c_2)(\dot{x}_2 - \dot{x}_1) + 2k_3x_2 \\ &\quad + (k_{12} + k_2)(x_2 - x_1) + k_{11}(x_2 - x_1)^3 + k_{12}\Delta = 0. \quad (|x_1 - x_2| > \Delta) \end{aligned} \tag{4b}$$

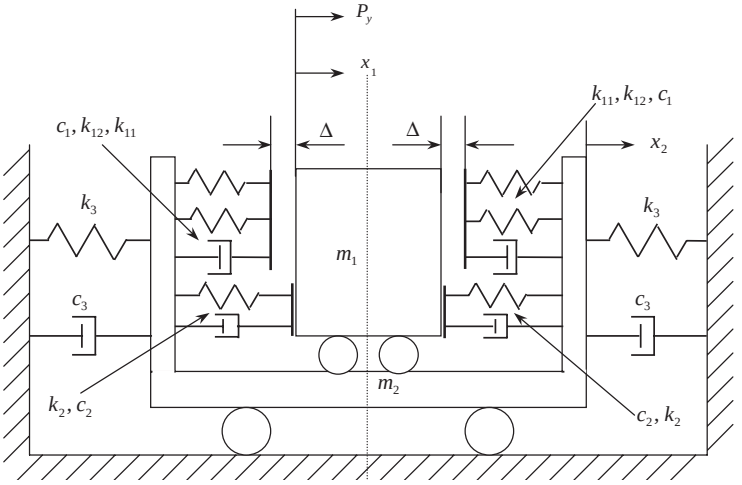

Fig. 5. A nonlinear dynamic model of the piston–cylinder system.

According to nonlinear dynamics [8,9], Eq. (4) expresses a hard stiffness problem with sectional linearity. By using the Runge–Kutta numerical integration procedure [8], the model can be evaluated with $P_y = 0$. Fig. 6 shows the calculated phase portraits of the vibration system with initial conditions of $\{x_1 = 0.0\,\text{mm},\ \dot{x}_1 = 0.4\,\text{m},\ x_2 = 0.0\,\text{mm},\ \dot{x}_2 = 0.0\,\text{m/s}\}$ (solid-line), as well as $\{x_1 = 0.0\,\text{mm},\ \dot{x}_1 = 0.2\,\text{m};x_2 = 0.0\,\text{mm},\ \dot{x}_2 = 0.0\,\text{m/s}\}$, (dotted line). For its first dof (the piston), there always is one stable focus at zero and for its second dof (the cylinder wall) there are at least two stable vortex points, with good repeatability. It is very well indicated from the diagrams that the developed model is stable and solvable for this application.

4. Numerical evaluations

Because the cubic term $k_{11}x^3$ exists in Eq. (4), polynomial fitting is introduced into the model, as well as the experimentally measured $P_y(t) = P_y$ [8]. Based upon this, numerical simulations of the slap-induced vibration response in terms of different working conditions of the engine are performed. Fig. 7 shows the dynamic responses of the piston and the cylinder wall excited by the slap impact. They demonstrate a similar abrupt process as anticipated above, especially at 4 major points A–D, where the displacement of the piston changes from positive to negative (or vice versa) and induces corresponding abrupt responses on the cylinder wall. Phase delays are obviously noticed between the vibration response and the dotted inner-cylinder excitation, mainly caused by the structural behaviour of this nonlinear system (damping and especially, the piston clearance).

Fig. 8 shows the simulated vibration response of the cylinder wall excited by the slap impacts and Table 1 lists the time of occurrence for every abrupt response, under different working conditions. In practice, these results are too expensive or sometimes impossible to obtain directly from experiments. From Figs. 8 (a) and (b) it is learnt that, under different rotating speeds, the abrupt slap response is not always identifiable as it is with the slap impact as discussed in Fig. 4.

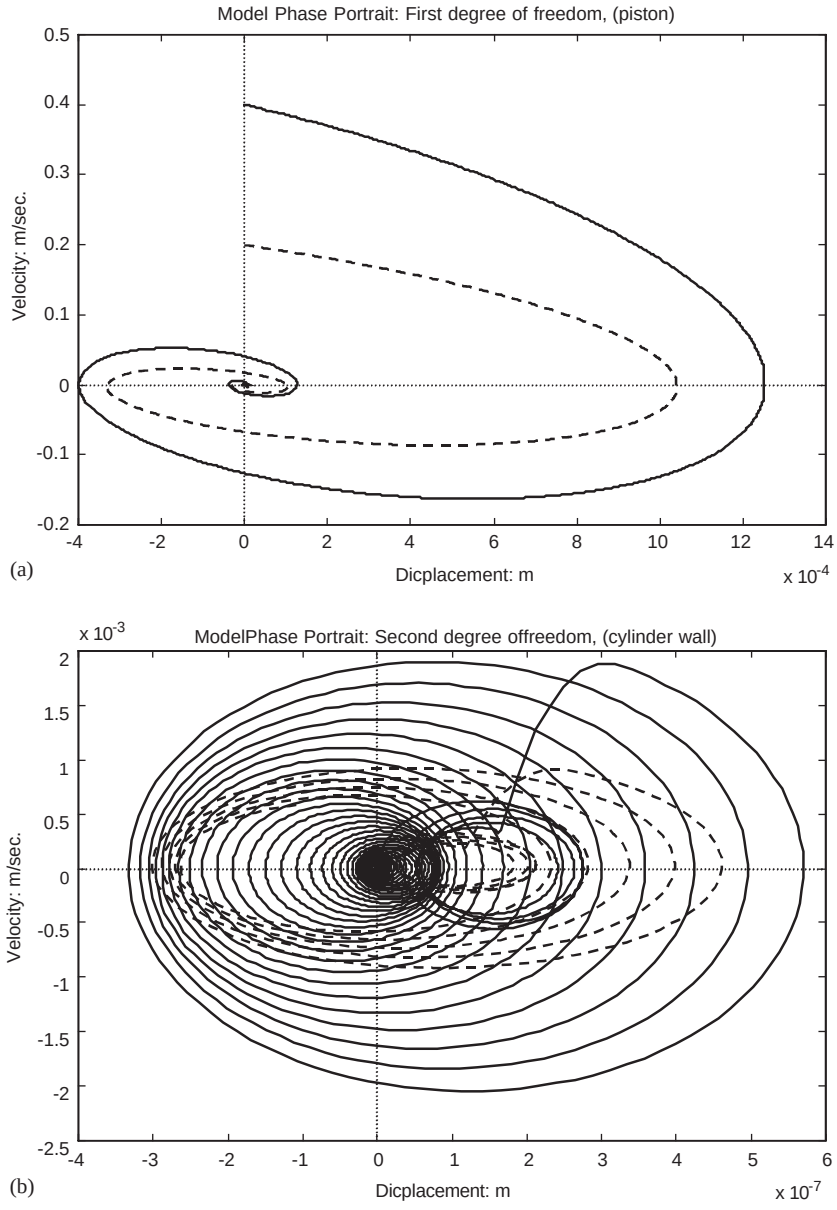

Fig. 6. Phase portrait of the piston–cylinder wall system: (a) piston assembly, (b) cylinder wall.

Especially for light-load and high-speed situations, the relatively long periodic oscillation of the first slap response often submerges the abrupt starting of the second one. Comparatively, relatively lower rotating speed and heavier load are more helpful in identifying the time of abrupt slap-induced vibration occurrence, especially, the 4 major points A–D.

Figs. 8(c) and (d) show how the slap-induced response changes regularly with different piston clearances. Under a constant rotating speed, phase delay of the slap-induced response

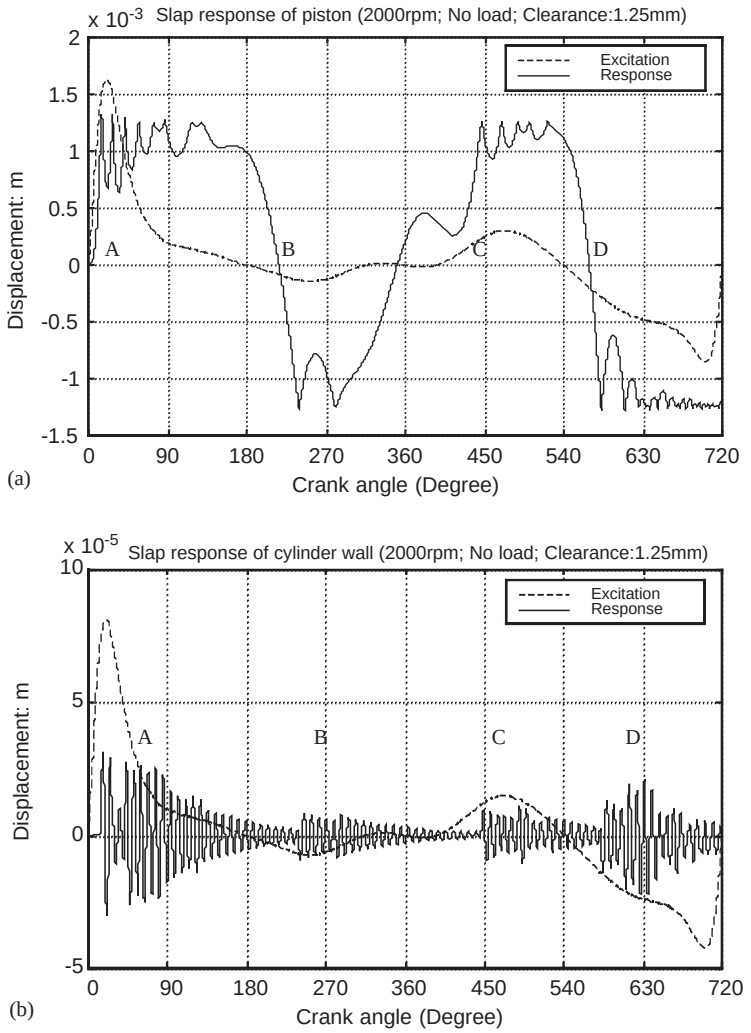

Fig. 7. Simulations of the slap-induced response: (a) vibration displacement of the piston, (b) vibration displacement of the cylinder wall.

increases exponentially with an increase of the piston clearance as is shown in the figures. Obviously, this reveals a dependent relationship between the slap-induced response and the piston clearance which has an important engineering implication. At the same time, in a theoretical sense, it gives a strong verification of the developed nonlinear model as expressed in Eq. (4).

By comparing the items listed in Table 1, a definite numerical estimate of the phase delay between the slap-induced response and the slap impact can be obtained, especially for the 4 major points A–D. Under low rotating speed and heavy load, a constant phase delay between them is maintained by the piston clearance and lubricant damping between the piston and the cylinder wall.

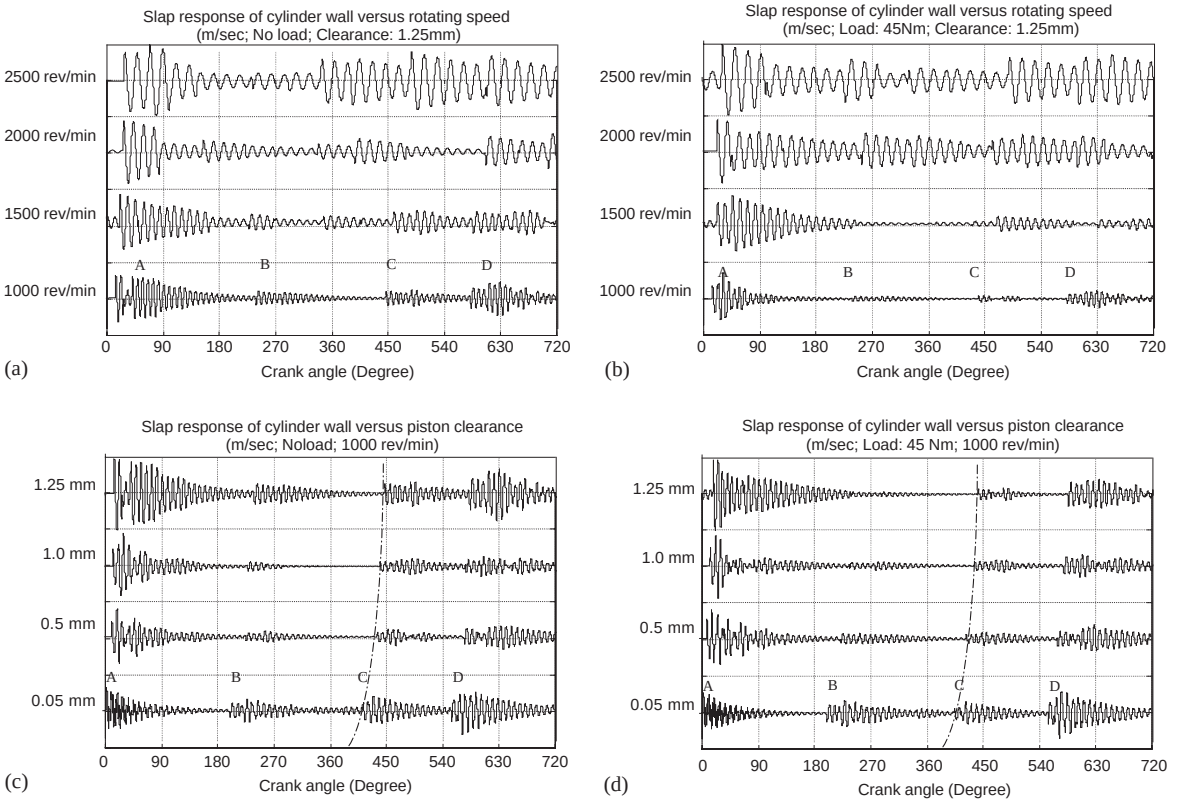

Fig. 8. Simulations under different working conditions: (a) under different rotational speeds (no external load), (b) under different rotational speeds (external load: 45 Nm), (c) with different piston clearances (no external load), (d) with different piston clearances (external load: 45 Nm).

5. Extraction of the slap-induced vibration signature

Although the above-mentioned simulation reveals a correlation between the piston-slap impact and the slap-induced vibration response, much difficulty still remains in extraction of these signature points from practically measured vibration signals and application of this approach to practical engineering. This is mainly caused by the severe reverberation and dispersion influences of the complicated engine structure. Considering this complex situation, the specially designed experimental scheme shown in Fig. 2 is introduced into this research and, furthermore, a specially designed fast wavelet-packet decomposing method is applied to the extraction.

5.1. Decomposition algorithm of the wavelet packet

According to the wavelet algorithm [10,11], the engine vibration signal $u(t)$ can be further represented as its wavelet decomposition form

$$u(t) = A_{J_2}u(t) + \sum_{j=J_1}^{J_2} D_j u(t) = \sum_{k\in Z} C_{J_2k}\varphi_{J_2k}(t) + \sum_{j=J_1+1,k\in Z}^{J_2} \psi_{jk}(t), \tag{5}$$

where $A_{J_2}u(t) = \sum_{k\in Z} C_{J_2k}\varphi_{J_2k}(t)$ represents the signal components, the frequencies of which are lower than 2^{-J_2}, whilst $D_j u(t) = \sum_{k\in Z}\psi_{jk}(t)$ represents the signal components the frequencies of which are between 2^{-j} and $2^{-(j-1)}$. Sampling point $j = J_1, \ldots, J_2 - 1$.

Further representing Eq. (5) in the combination form of its low-pass average-filter H and high-pass differential-filter G, it can be expressed as follows:

$$C_{j+1} = HC_j, \quad D_{j+1} = GC_j, \quad j = J_1, \ldots, J_2 - 1. \tag{6}$$

Actually, Eq. (6) represents a filtering procedure by a series of orthogonal conjugate filters H and G: firstly, decomposing the originally measured vibration signal $u(t)$ according to Eq. (5), secondly, based on obtained knowledge of the signal composition, filtering and reconstructing a new series of $\tilde{C}_{J2}$ and $\tilde{D}_j$ $(j = J_2, J_2 - 1, \ldots, J_1 + 1)$, and finally, getting a new noise-free signal series $\tilde{u}(t) = \sum_{k\in Z}\tilde{C}_{J_2k}\varphi_{J_2k}(t)$. According to this procedure and supposing $C_{i,j}$ to be its ith by jth scale factor, the normally used decomposition algorithm of the wavelet packet proceeds with its two-to-one sampling is as follows:

$$\begin{gathered} C_{1,0}(t) = u(t), \quad C_{2i-1,j}(t) = HC_{i,j-1}(t), \quad C_{2i,j}(t) = GC_{i,j-1}(t), \\ t = 1, \ldots, 2^{J-j}; \quad i = 1, \ldots, 2^j; \quad j = 1, \ldots, J; \quad J = \log_2 N. \end{gathered} \tag{7}$$

After this decomposition procedure, a reasonable sorting work [10,11] must be done to get the function of GC^{-1}, so as to get an orderly frequency-divided series. Its deductive expression is sketched in Fig. 9 and detailed as follows:

$$\begin{gathered} GC^{-1}(0) = 0, \quad GC^{-1}(1) = 1, \\ GC^{-1}(2n) = 2GC^{-1}(n), \ GC^{-1}(n) \text{ be even}; \\ GC^{-1}(2n) = 2GC^{-1}(n) + 1, \ GC(n) \text{ be odd}; \\ GC^{-1}(2n+1) = 2GC^{-1}(n) + 1, \ GC^{-1}(n) \text{ be even}; \\ GC^{-1}(2n+1) = 2GC^{-1}(n), \ GC^{-1}(n) \text{ be odd}. \end{gathered} \tag{8}$$

5.2. Fast reconstruction algorithm of the wavelet packet

As shown in Fig. 9 and Eq. (8), above layer-to-layer decomposition brings equally distributed frequency bands. However, in this paper only a few important frequency bands will be used in the calculation and discussion. A fast reconstruction algorithm can be therefore arranged as sketched in Fig. 10 and detailed as follows:

(1) Choosing the suitable orthogonal conjugate filters H and G.
(2) Selecting the decomposing layer J and routes (Fig. 10). If the length of the original signal $u(t)$ equals 2^N, its sampling frequency is f_{sm} and we are only interested in the m frequency bands at the jth layer; we can get it as $\{n_1, n_2, \ldots, n_m\}$.
(3) Decomposing $u(t)$ by using Eq. (8), a new serial can be obtained as

$$\begin{gathered} nC_{i,J}(t) = C_{i,J}(t), \quad i = \{n_1, n_2, \ldots, n_m\}; \\ nC_{i,J}(t) = 0, \quad i \neq \{n_1, n_2, \ldots, n_m\}. \end{gathered} \tag{9}$$

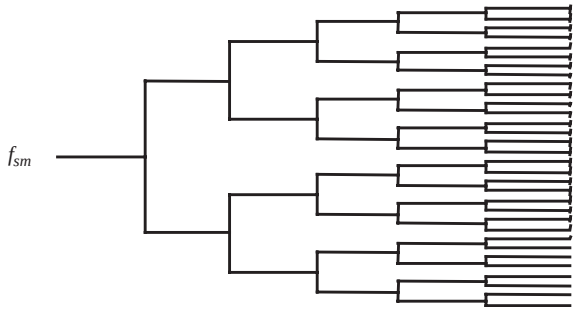

Fig. 9. Layer-to-layer decomposing algorithm of the wavelet packet.

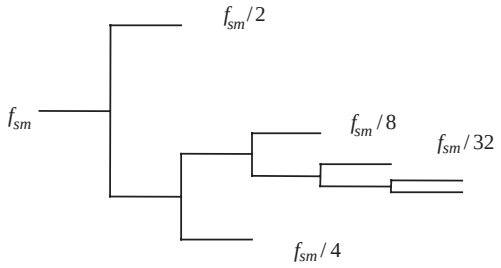

Fig. 10. Fast reconstruction of the wavelet packet.

(4) Reconstructing the original signal with interested frequency components:

$$\tilde{C}_{i,j}(t) = 2\left[H^* \tilde{C}_{2i-1,j+1}(t) + G^* \tilde{C}_{2i,j+1}(t)\right] \tag{10}$$

A simulation result of the signal $u(t) = \sin(2\pi f_1 t) + \sin(2\pi f_2 t) + n(t)$ is as shown in Fig. 11, to verify the above algorithm. Here $f_1 = 700\,\text{Hz}, f_2 = 60\,\text{Hz}$ and $n(t)$ is a Gaussian noise. Obviously, the fast wavelet-packet reconstruction algorithm can perfectly extract the interested frequency components from a complex signal with much less power-leaking and aliasing effects than the commonly used FIR filters.

5.3. Extraction of the slap-induced vibration signature

As a brief experimental verification of the above-mentioned methodologies, Fig. 12 shows some practically measured and reconstructed slap-induced time-domain vibration signals of the 6190Z_LC diesel engine. Figs. 12(a) and (b) are from an old engine and Fig. 12(c) is from a brandly new one. In the figure, CH1 represents the practically measured inner-cylinder combustion pressure, while CH2–CH4 represent the reconstructed time-domain vibration signals, respectively, measured at the middle, lower parts of the major-thrust side and the middle of the

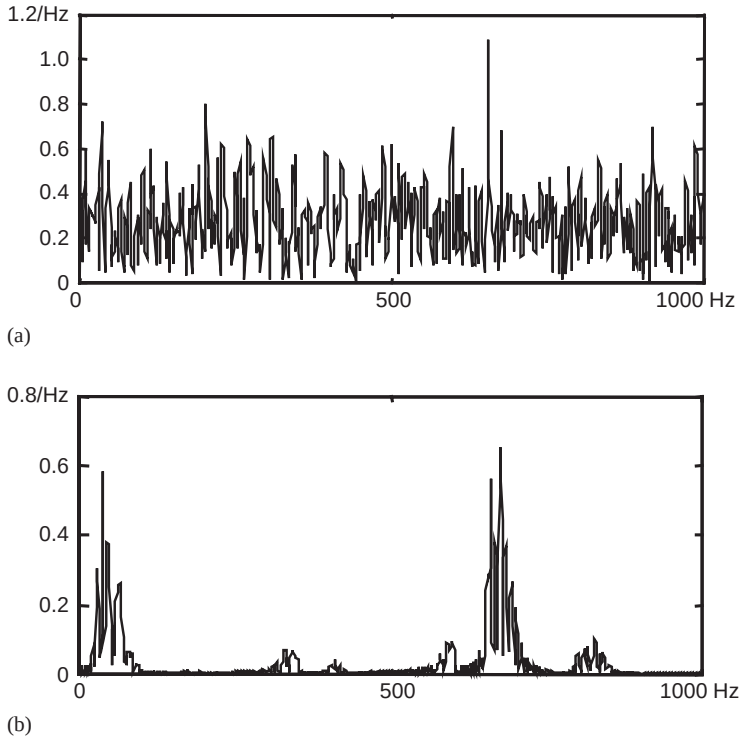

Fig. 11. Simulation of the fast wavelet-packet reconstruction algorithm: (a) spectrum of the original signal, made from two sinw waves at 700 and 60 Hz, immersed in Gaussian noise, (b) spectrum of the reconstructed signal.

non-major-thrust side of the cylinder wall along its axial direction (compared with the dotted side-thrust force). Compared with the complex waveform shown in Fig. 1, Fig. 12 clearly shows every occurrence and intensity of the slap-induced impact. Comparison between Figs. 12(a–c), as well as the relevant items listed in Table 1, also reveals a good coincidence in the slap-induced response effects. For example, in Figs. 12(a) and (b), compared with the weaker combustion-induced response point A, points B–D are irregularly distributed, while in Fig. 12(c), compared with the more abrupt and stronger combustion-induced response point A, the other two signature points C and D mainly represent the effects of combustion force, regularly distributed and demonstrate the difference between the two engines' working conditions.

6. Conclusions

As a new attempt and preliminary investigation, this paper presents a new idea for the reciprocating engine's dynamic analysis and working condition monitoring. By correlating the piston-slap phenomenon with the slap-induced vibration response, an applicable approach for the engine's inner-cylinder vibration simulation and working condition monitoring is presented.

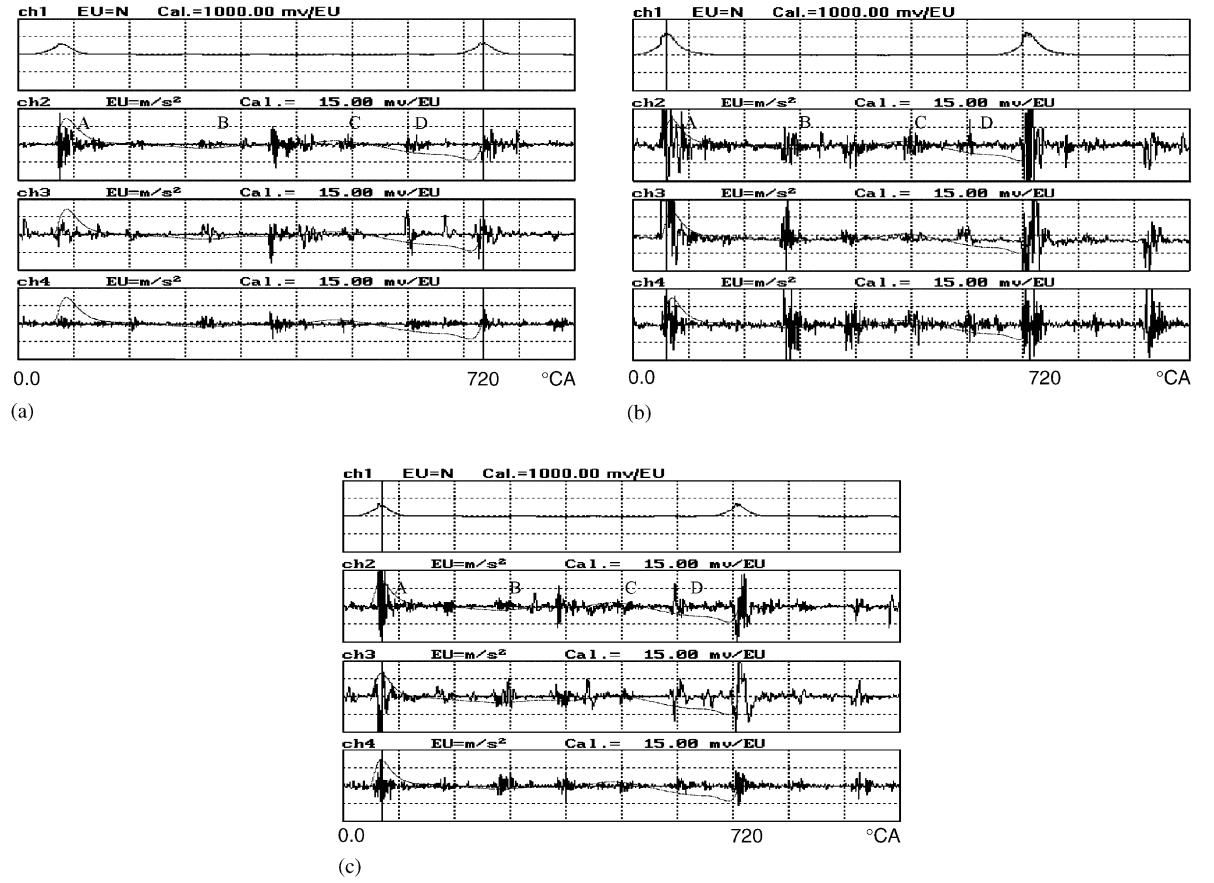

Fig. 12. Experimentally measured and reconstructed slap-induced vibration: (a) more effects from the inertia force (1000 rev/min), (b) more effects from the inertia force (1500 rev/min), (c) more effects from the combustion force (1500 rev/min).

From theoretic derivation, dynamic modelling and simulation, up to practical experimental design and signal reconstruction processing, the following conclusions are obtained:

(1) As a new attempt, the idea of applying the correlation between the inner-cylinder piston-slap impact and the slap-induced vibration response to simulate the engine's inner-cylinder dynamic behaviour and evaluate its performance or working condition is proven to be appropriate and applicable.
(2) Theoretical description on the piston-slap mechanism is proven to be reasonable, respectively, by the analytical simulation and specially designed experiment. This understanding is helpful in further investigation into the piston-slap phenomenon and relevant dynamic problems.
(3) The tdof non linear dynamic model developed in this paper is also proven to be reasonable and suitable in describing the mutually dependent correlations of the inner-cylinder excitations, piston–cylinder wall structural properties, as well as its vibration response,

respectively, by the analytical simulation and specially designed experiment. Although this model is simple and brief (for example, the rotional freedom of the piston assembly as well as the inner-cylinder thermal effect is not considered), it supplies a framework for similar system modelling, as well as a hint in understanding the mutualcorrelation of the inner-cylinder piston-slap impact and slap-induced response. It will also be very helpful in further investigation into the engine dynamic problems.

(4) In the sense of engineering application, the specially designed experimental scheme and fast wavelet-packet signal processing method have proven to be successful in this research. Practical application of these methods in the $6190Z_LC$ diesel engine experiments verifies their suitability and practicality for engineering use.

Acknowledgements

This work was sponsored by the NSFC (Approved No. 59775024) and the K.C. Wong Education Foundation in Hong Kong.

References

[1] R.A. Collacot, *Mechanical Fault Diagnosis and Condition Monitoring*, UKM Publications, England, 1982.
[2] J.T. Kim, R.H. Lyon, Cepstral analysis as a tool for robust processing, deverberation and detection of transients, *Journal of Mechanical System and Signal Processing* 6 (1) (1992) 1–15.
[3] R.H. Lyon, *Machinery Noise and Diagnostics*, Butterworths, London, 1987.
[4] C. Cemple, *Vibroacoustic Condition Monitoring*, Ellis Horwood, Chichester, 1994.
[5] N.B. Jones, A review on condition monitoring and fault diagnosis for diesel engines, in: *Condition Monitoring'97*, National Defence Industry Press, P.R. China, March 1997, pp. 221–242.
[6] Z. Geng, On the random vibration behaviours and dynamic diagnosis of reciprocating machines, *ICVE'98*, Dalian, P.R. China, August 1998, pp. 195–202.
[7] Z. Geng, Techniques applicable to the non-stationary vibro-acoustic analysis and fault diagnosis of reciprocating machinery, *Journal of Mechanical Engineering* 32 (4) (1996) 56–62.
[8] M. Cartmell, *Introduction to Linear, Parametric, and Nonlinear Vibrations*, Chapman & Hall, London, 1990.
[9] J.P. Den Hartog, *Mechanical Vibration*, McGraw-Hill, London, 1968.
[10] J. Aguirre, et al., Basis of wavelets and atomic decompositions of $H^1 \to (R^n)$ and $H^1 \to (R^n \times R^n)$, *Proceedings of the American Mathematical Society* 111 (3) (1991) 683–693.
[11] O. Rioul, P. Duhamel, Fast algorithm for discrete and continuous wavelet transforms, *IEEE Transactions on Information Theory* 38 (1992) 569–586.